ADVANCED MATERIALS
www.advmat.de

www.MaterialsViews.com

Hierarchically Tunable Helical Assembly of Achiral Porphyrin-Incorporated Alkoxysilane

*Xuemei Sun, Longbin Qiu, Zhenbo Cai, Zhenyu Meng, Tao Chen, Yunfeng Lu, and Huisheng Peng**

Helical assembly is a common phenomenon in nature. The most well-known examples are double helices formed by DNA and α-helical motives in proteins. These biopolymers adopt helical conformations due to molecular information present in their building blocks, i.e., the helices demonstrate distinct functions from individual components.[1] Drawing from nature, scientists have shown increasing interest into this synthetic strategy and have explored various helical assemblies at the nanoscale.[2–6] Assembly mainly produces first-level helical structures based on chiral precursors. However, helical structures of various biomacromolecules, such as DNA, are created through non-covalent interactions among achiral building blocks. In addition, helical superstructures may be further formed from the first-level helices. A typical helical superstructure based on self-assembly is the tobacco mosaic virus.[7] Individual protein molecules of this virus spontaneously form a right-handed helix when mixed with viral DNA molecules. By deliberately designing building blocks and controlling the assembly process, it may be available to construct hierarchically biomimetic systems with helical superstructures and intriguing functionalities.

Due to their unique flat and conjugated central tetrapyrrole macrocycle, porphyrin derivatives have been widely investigated as model molecules in self-assembly.[8,9] For instance, porphyrin can be incorporated into an inorganic framework, such as silica, to produce hybrid materials,[10,11] and various nanometer- and micrometer-sized superstructures have been described from porphyrin assemblies, including solid materials, spheres, rods, and fibers.[11–15] Herein, we discover a novel assembly approach to construct hierarchically tunable helical superstructures based on an achiral porphyrin-incorporated alkoxysilane (PIA) in which four triethoxysilane groups are grafted to the central macrocycle (**Scheme 1**). The PIA superstructures can be tuned from film, rice, spindle, ribbon, to fiber in morphology and from non-helicity to helicity in structure, which spans nano- to macroscopic scales. These superstructures also exhibit excellent optoelectronic, electronic, and thermal properties. In addition, this construction may be also extended to other conjugated molecules, and represents a paradigm to design and build a family of functional materials.

PIA was synthesized from 4,4′,4″,4‴-(21H,23H-porphine-5,10,15,20-tetrayl) tetrakis (benzoic acid) and γ-isocyanatopropyltriethoxysilane. Purified PIA was then dissolved in tetrahydrofuran (THF) at a concentration of 10 mg mL^{-1}. Similar to other bridged silsesquioxianes,[16,17] direct coating of PIA/THF solution on glass substrates produced uniform thin films after fast evaporation of solvents (typically several seconds). **Figure 1**a shows a scanning electron microscopy (SEM) image of a film with crystal-like structure. In order to slow and control evaporation speeds, PIA/THF solution was carefully dropped to an acidic aqueous solution (pH of approximately 4) to form two layers, with PIA solution being the top

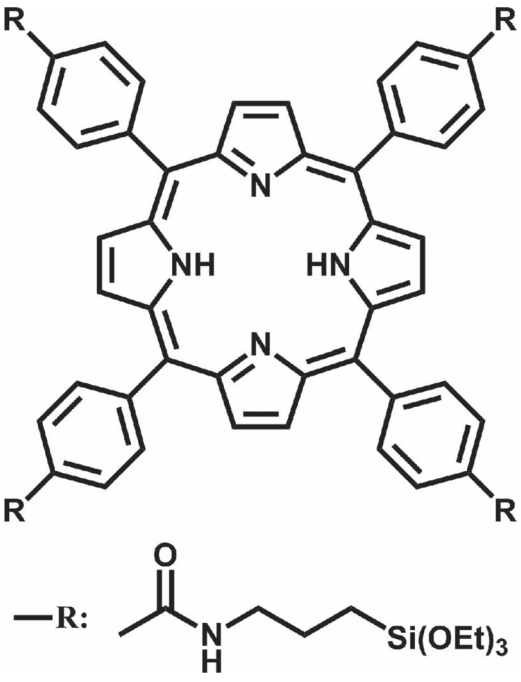

Scheme 1. Chemical structure of porphyrin-incorporated alkoxysilane (PIA).

X. M. Sun, L. B. Qiu, Z. B. Cai, Z. Y. Meng, T. Chen, Prof. H. S. Peng
State Key Laboratory of Molecular Engineering of Polymers
Department of Macromolecular Science and Laboratory of Advanced Materials
Fudan University
Shanghai 200438, China
E-mail: penghs@fudan.edu.cn
Prof. Y. F. Lu
Department of Chemical and Biomolecular Engineering
University of California Los Angeles
Los Angeles, CA 90095, USA

DOI: 10.1002/adma.201200422

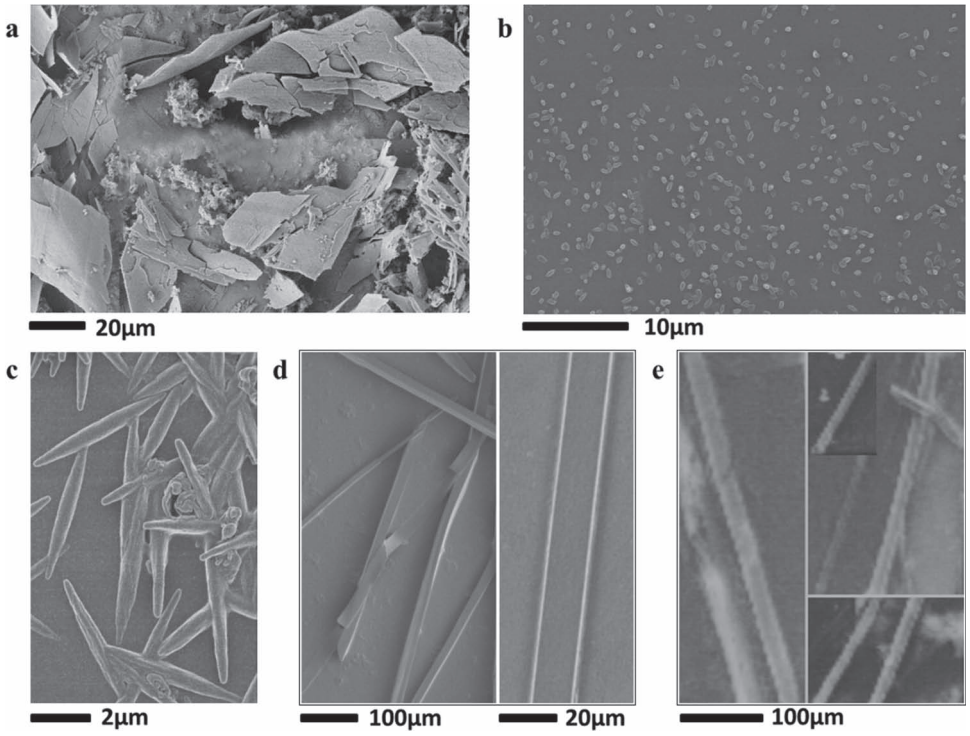

Figure 1. SEM images of PIA superstructures with different morphologies: a) film, b) rice, c) spindle, d) ribbon, and, e) fiber.

layer. Evaporation speeds of solvents were tuned by varying the vapor pressure above PIA solution at room temperature. Interestingly, PIA molecules assembled into nanometer-sized rice-shaped aggregates, micrometer-sized spindle-shaped aggregates, macroscopic ribbons, and macroscopic helical fibers with decreasing evaporation speeds from about 20 min to over 10 h, 4–6 d, and 3-4 weeks, respectively. Figure 1b shows rice-shaped aggregates with average diameter of approximately 400 nm and length of approximately 800 nm. Figure 1c shows spindle-shaped aggregates with diameter between 550 and 700 nm and length between 4.3 and 5.6 μm. Figure 1d shows ribbons with width of approximately 20 μm and length up to millimeter-scale. Figure 1e shows helical fibers with diameter of tens of micrometers and length up to centimeter-scale. Although film and ribbon have been widely explored in the self-assembly of conjugated organic building blocks, including porphyrin derivatives, the other morphologies have been rarely observed. In addition, simultaneous control of assemblies with such a wide variety of tunable morphologies – from film to rice, spindle, ribbon, and fiber, and sizes from nanometer to micrometer, millimeter, and centimeter – has not been realized previously.

Structures of assemblies with different morphologies were analyzed by X-ray diffraction (XRD), atomic force microscopy (AFM), transmission electron microscopy (TEM), and circular dichroism (CD). A lamellar mesostructure with *d*-spacing of 2.10 nm (corresponding to the diagonal length of a PIA molecule) was mainly found for thin films, while a closely packed hexagonal mesostructure with similar *d*-spacing was observed for the other morphologies, such as fiber (**Figure 2**). Figure 2a shows representative small-angle XRD patterns of the above two organizations, with two peaks of (100) and (300) observed for lamellar mesostructure and three peaks of (100), (110), and (300) for hexagonal mesostructure. The lamellar and hexagonal mesostructures was further confirmed by high-resolution TEM (Figure 2b) and AFM (Figure 2c), respectively.

Generally, porphyrin derivatives with chiral side-chains are designed to stack helically into nano-columns or fibers during molecular assembly.[13] In the case of achiral side-chains, certain helical stacking has been recently realized through external inductions, such as directional stirring and use of a chiral polymer template.[18,19] Here we are interested in the possibility of achieving helical assembly of achiral molecules without external induction. The helical stacking or assembly is typically analyzed by circular dichroism (CD) characterization, and PIA film was first carefully investigated by CD. No CD signals were detected for PIA solutions in a wide variety of concentrations, and no CD signals were found in PIA film either (Figure 2e). It seems that PIA molecules randomly stack, similar to typical achiral conjugated organic building blocks such as perylenediimide-incorporated alkoxysilane, without external inductions.[20] Unexpectedly, helical stacking of PIA molecules was clearly observed in the film morphology under high-resolution TEM. Figure 2d shows the side-view of two stacks with a helical angle of approximately 40°. Although these two stacks are right-handed, the probability of forming right- and left-handed structures should be the same.[21–24] Therefore, only racemic stacks are produced macroscopically, which explains the phenomena that both PIA solution and film are CD-silent.

The helical stacking of PIA molecules was also found in rice, spindle, ribbon, and fiber-shaped assemblies under high-resolution TEM. Figure S1 (Supporting Information) shows a

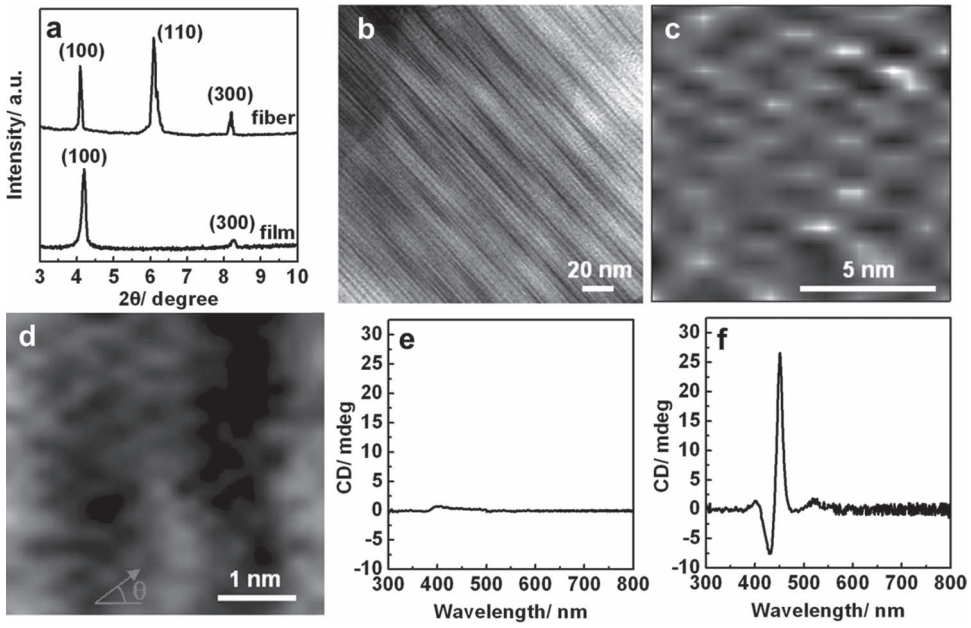

Figure 2. Structure characterizations of PIA assemblies: a) XRD patterns of film and fiber, with *d*-spacings of 2.10 and 2.16 nm, respectively, b) high-resolution TEM image showing a lamellar mesostructure of a film, c) AFM image showing a hexagonal mesostructure of a fiber, d) high-resolution TEM side-view image of PIA stacks showing a helical angle of approximately 40° in a fiber, e) CD spectrum of a film, and, f) CD spectrum of a fiber.

representative TEM image similar to those for the film. Wide-angle XRD had been also widely used to investigate the stacking format of porphyrin derivatives.[25,26] Different from the non-helical stacking with an average interplannar distance of 0.42 nm,[26] Figure S2 shows a typical wide-angle XRD pattern for the PIA fiber with an interplanar distance of 0.74 nm, which also confirms the helical stacking of PIA molecules.[25] Figure 2f further shows a typical CD spectrum with a negative peak at a shorter wavelength and a positive peak at a longer wavelength, which indicates a dominating anti-clockwise chirality.[27] Since right- and left-handed nano-stacks of PIA molecules are formed with the same probability, the CD signals must be produced by their hexagonal winding along a preferred direction. Generally, helical symmetry is broken by external inductions, including chemical reaction, directional stirring, and polarized light irradiation for achiral building blocks.[22,23] Here no external inductions were introduced, so this chirality may be due to spontaneous symmetry breaking at the air/solution interface.[22–24] On the other hand, a weaker positive peak at the shorter wavelength and a weaker negative peak at the longer wavelength were also observed in the CD spectrum for the fiber (Figure S3), which indicates the formation of a clockwise chirality, albeit dominated by the anti-clockwise chirality.

The helical stacking of achiral PIA nanodisks and further organization of the resulting nano-stacks are schematically shown in **Figure 3**. Atoms in the porphyrin macrocycle stay in the same plane, with phenyl rings perpendicular to the porphyrin plane (Figure 3a).[18] Here planar porphyrin macrocycles favor formation of molecular stacks, while four branches with perpendicular phenyl rings lead to rotation of PIA molecules for a helical organization (Figure 3b).[21] Primary driving forces include π–π interactions among porphyrin macrocycles, hydrogen bonding among amide moieties (–CONH–), and van der Waals forces among side-chains.[25] The rotary directions of nano-stacks are determined by the stacking direction of the second PIA molecule relative to the first one, i.e., a clockwise stacking produces left-hand helices, while an anti-clockwise stacking produces right-hand helices. Based on the molecular structure of PIA, we obtain the diameter of nano-stacks to be approximately 2 nm, which is consistent with XRD results, as well as AFM and TEM images (Figure 2). In the case of a film, these nano-stacks formed a lamellar structure as a fast evaporation of solvent did not allow for their optimal arrangement. For rice, spindle, ribbon, and fiber with decreasing evaporation speeds, UV-vis spectroscopy and Fourier transform infrared (FTIR) spectroscopy were used to trace the stacking of PIA molecules.

UV-vis spectroscopy was performed to compare the optoelectronic properties of PIA assemblies with different morphologies and structures (Figure S4). PIA/THF solution shows a sharp absorption peak at 418 nm for the Soret band and four absorption peaks at 513, 548, 591, and 648 nm for the Q bands.[25,28] After formation of assemblies with morphologies from film, rice, spindle, ribbon, to fiber, both the Soret and Q bands exhibit red shifts with increasing peak intensities. For instance, the peak of the Soret band shifts to 444 nm and four peaks for the Q bands shift to 521, 556, 595, and 649 nm in film, respectively; the peak of the Soret band and four peaks of the Q bands further shift to 445 nm and 542, 562, 600, and 653 nm in fiber, respectively. It is well known that these red shifts are associated with more efficient stacking of PIA molecules and more ordered packing of PIA nano-fibers.[16,29]

Silane groups are designed to be chemically bonded to four grafts in porphyrin molecules, and they can easily go on, via

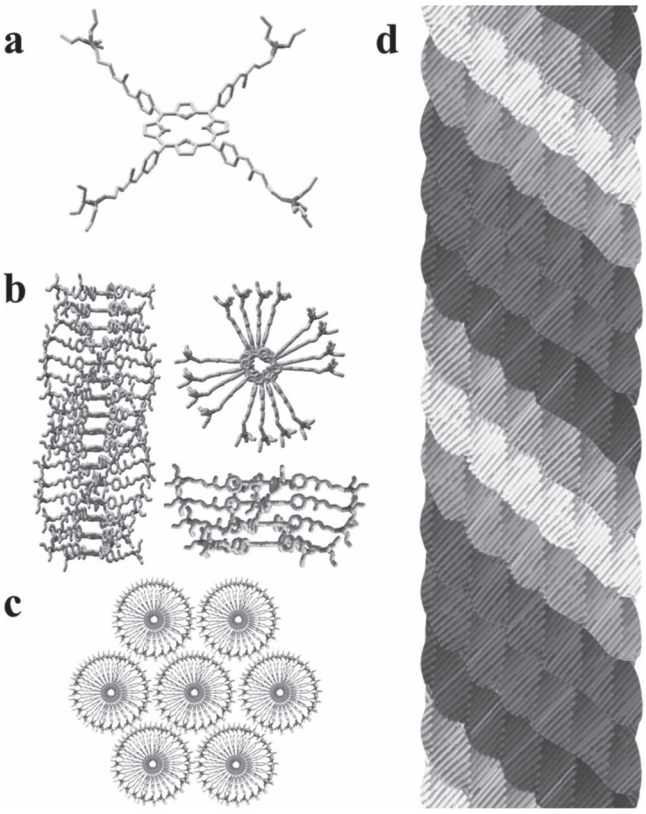

Figure 3. Schematic illustration of PIA assembling processes: a) structure of a PIA molecule after hydrolysis, b) side view of a helical PIA stack, c) top view of a hexagonal arrangement of PIA stacks, and, d) PIA nano-stacks wind clockwise to form left-hand helical nanostructure or superstructure. For visual clarity, hydrogen atoms are omitted in (b and c), and the nano-stacks in (d) are drawn with different shading.

hydrolysis and condensation reactions, to produce highly stable and robust silica network.[25,30] The above reactions were confirmed by FTIR spectroscopy. As shown in Figure S5, the characteristic peaks of Si–OEt at 1102 and 1077 cm^{-1} disappear, while a broad Si–O–Si stretching at 1058 cm^{-1} appears, suggesting the formation of covalently bonded silica/porphyrin nanocomposites.[11,31] In addition, these porphyrin/silica hybrid materials also showed excellent thermal stability. For instance, the decomposition temperature was improved to 800 °C in air, much higher than the 500 °C of pure powder of 4,4′,4″,4‴-(21H,23H-porphine-5,10,15,20-tetrayl) tetrakis (benzoic acid; see Figure S6).[13] Furthermore, due to conjugated macrocycles, porphyrin/silica hybrid materials were further carbonized typically at 750 °C in argon, as confirmed by Raman spectroscopy. Figure S7a compares Raman spectra of a ribbon before and after carbonization. Two characteristic peaks at 1593 cm^{-1} for the G band and 1348 cm^{-1} for the D band are observed to show the graphitic structure in the carbonized ribbon,[32,33] while the peaks corresponding to the PIA ribbon prior to carbonization disappear. The inserted optical images in Figure S7a show the ribbon before and after carbonization, which indicates that both the morphology and the size of the ribbon have been well retained. Nitrogen was doped into carbon lattices after carbonization.[19]

Based on the UV-vis spectroscopy and FTIR spectroscopy, we can conclude that, in the cases of rice, spindle, ribbon, and fiber, obtained with decreasing evaporation speed, nano-stacks have increasing time to wind closely and hexagonally into more-ordered structures through cooperative interactions among PIA side-chains (Figure 3c). Helical winding and hexagonal organization of PIA nano-stacks with decreasing evaporation speed also favors formation of aggregates with increasing aspect ratios and more highly ordered structures. In the case of rice, spindle, and ribbon, with relatively rapid evaporations, PIA nano-stacks hexagonally wind into helical nanostructure but cannot grow into a macroscopically helical superstructure.[28,31] For much slower evaporation, which allows for an optimal arrangement, helical nanostructures continue growing into larger helical superstructures, i.e., macroscopic fibers (Figure 3d).

Considering the highly stacked structure of porphyrin moieties, we also investigated the electronic properties of the nanocomposite. The as-synthesized nanocomposite typically showed an electrical conductivity on the level of 10^{-7} S cm^{-1} at room temperature. The electrical conductivity can be improved by three orders of magnitude after complexation of metal ions into the center of conjugated porphyrin macrocycles. For instance, the nanocomposite complexed with zinc ions exhibited a conductivity of 5×10^{-4} S cm^{-1}.

Nitrogen-doped carbon nanomaterials represent a family of metal-free catalysts in fuel cells.[34–37] They have been reported to exhibit excellent electrocatalytic activity for oxygen-reduction reactions because of their unique electronic properties, derived from the conjugation between nitrogen lone-pair electrons and the graphene system. Here we measured the electrochemical performance of carbonized ribbons through an electrochemical work station using a rotating-disk electrode. Carbonized ribbons were first pasted onto the rotating disk electrode, and cyclic voltammogram curves were then obtained in 0.1 M KOH solution saturated with O_2 at a scan rate of 100 mV s^{-1} and an electrode rotation rate of 100 rpm. The current density easily achieved 1.60 mA cm^{-2} at –0.47 V (Figure S7b), compared with 1.1 mA cm^{-2} at –0.2 V for a platinum/carbon electrode under the same conditions.[37] Obviously, carbonized assemblies exhibit a good electrocatalytic activity for oxygen reduction.

In summary, we have developed a general assembly approach to construct hierarchically tunable helical superstructures by using achiral bridged silsesquioxane incorporated with conjugated macrocycle. The resulting superstructures can be controlled over a wide range of morphologies and tuned from non-helical to helical structures at multiscale by simply varying the evaporation speed to control the assembly dynamics. Due to the combined advantages of conjugated macrocycle and grafted silsesquioxane groups, these superstructures exhibit excellent optoelectronic, electrical, and thermal properties.

Experimental Section

Synthesis of Porphyrin-Incorporated Alkoxysilane: 4,4′,4″,4‴-(21H,23H-porphine-5,10,15,20-tetrayl) tetrakis (benzoic acid) (0.1 mmol) and γ-isocyanatopropyltriethoxysilane (0.4 mmol) were added to tetrahydrofuran (10 mL) in a multinecked flask. The flask was repeatedly evacuated and flushed with nitrogen gas. The mixture was stirred for several minutes under nitrogen atmosphere, and then refluxed at 80 °C in an oil bath

overnight. The reaction was stopped by cooling mixture solution to room temperature. The final product was washed with petroleum ether to remove excess γ-isocyanatopropyltriethoxysilane. The two precursors, 4,4′,4″,4‴-(21H,23H-porphine-5,10,15,20-tetrayl) tetrakis (benzoic acid) and γ-isocyanatopropyltriethoxysilane, were ordered from Sigma Aldrich and used as received.

Assembly of PIA Molecules: The purified PIA was dissolved in THF with concentration of 10 mg mL^{-1}. After ultrasonic treatment for 10 min, the solution (10 mL) was filtered with nylon membrane (pore diameter of 0.22 μm), followed by addition of approximately 20 μL of 0.1 M HCl. For the preparation of film, the final solution was directly coated on glass substrates followed by evaporation of solvents at room temperature. For the preparation of rice, spindle, ribbon, and fiber, the final solution was slowly dropped to the top of water (pH of approximately 4) in a vial with a volume of 20 mL. Typically, the volumes of water and the solution were 4 and 10 mL, respectively, and a clear interface was observed between final solution and water. Evaporation of solvents was performed at room temperature, and evaporation speeds were controlled by varying vapor pressure in the vial.

Characterization: Assembly morphologies were characterized by fluorescence microscopy (Olympus BX51) and scanning electron microscopy (S-4800, operated at 1 kV), Assembly structures were analyzed by X-ray diffraction (XRD, D8 ADVANCE and DAVINCI.DESIGN, Ni-filtered Cu Kα radiation at $\lambda = 0.15418$ nm, operated at 40 kV and 40 mA), transmission electron microscopy (JEOL 2010 operated at 120 kV), atomic force microscopy (Q-Scope 250 Quesant), and circular dichroism (CD) spectra (JASCO J-715 spectrapolarmeter). UV-visible spectra were recorded using a Shimadz U-3150 spectrophotometer. FTIR spectra were recorded using a Shimadz IRPrestige-21 spectrometer. The electrical conductivity was obtained from a Solartron 1260 gain phase analyzer in the frequency range 10 to 1×10^7 Hz.

Supporting Information

Supporting Information is available from the Wiley Online Library or from the author.

Acknowledgements

This work was supported by NSFC (20904006, 91027025), MOST (2011CB932503, 2011DFA51330), STCSM (1052nm01600, 11520701400), MOE (NCET-09-0318), CPSF (20110490888), and Fok Ying Tong Education Foundation.

Received: January 30, 2012
Revised: March 15, 2012
Published online: April 27, 2012

[1] H. Engelkamp, S. Middelbeek, R. J. M. Nolte, *Science* **1999**, *284*, 785.
[2] R. Lauceri, A. Raudino, L. M. Scolaro, N. Micali, R. Purrello, *J. Am. Chem. Soc.* **2002**, *124*, 894.
[3] L. Brunsveld, J. A. J. M. Vekemans, J. H. K. K. Hirschberg, R. P. Sijbesma, E. W. Meijer, *Proc. Natl. Acad. Sci. USA* **2002**, *99*, 4977.
[4] V. Percec, M. Peterca, T. Tadjiev, X. Zeng, G. Ungar, P. Leowanawat, E. Aqad, M. R. Iman, B. M. Rosen, U. Akbey, R. Graf, S. Sekharan, D. Sebastiani, H. W. Spiess, P. A. Heiney, S. D. Hundson, *J. Am. Chem. Soc.* **2011**, *133*, 12197.
[5] V. Percec, S. D. Hundson, M. Peterca, P. Leowanawat, E. Aqad, R. Graf, H. W. Spiess, X. Zeng, G. Ungar, P. A. Heiney, *J. Am. Chem. Soc.* **2011**, *133*, 18479.
[6] E. Yashima, K. Maeda, Y. Furusho, *Acc. Chem. Res.* **2008**, *41*, 1166.
[7] R. E. Franklin, *Nature* **1955**, *175*, 379.
[8] L. L. Li, C. J. Yang, W. H. Chen, K. J. Lin, *Angew. Chem. Int. Ed.* **2003**, *42*, 1505.
[9] K.-J. Lin, *Angew. Chem. Int. Ed.* **1999**, *38*, 2730.
[10] H. Qiu, Y. Inoue, S. Che, *Angew. Chem. Int. Ed.* **2009**, *48*, 3069.
[11] T. Kishida, N. Fujita, K. Sada, S. Shinkai, *Langmuir* **2005**, *21*, 9432.
[12] S. B. Lei, C. Wang, S. X. Yin, H. N. Wang, F. Xi, H. W. Liu, B. Xu, L. J. Wan, C. L. Bai, *J. Phys. Chem. B* **2001**, *105*, 10838.
[13] Y. F. Qiu, P. L. Chen, M. H. Liu, *J. Am. Chem. Soc.* **2010**, *132*, 9644.
[14] S. J. Lee, J. T. Hupp, S. T. Nguyen, *J. Am. Chem. Soc.* **2008**, *130*, 9632.
[15] J. H. Xiao, Z.Y. Yin, H. Li, Q. Zhang, F. Boey, H. Zhang, Q. C. Zhang, *J. Am. Chem. Soc.* **2010**, *132*, 6926.
[16] H. Peng, Y. F. Lu, *Adv. Mater.* **2008**, *20*, 797.
[17] J. J. E. Moreau, B. P. Pichon, M. W. C. Man, C. Bied, H. Pritzkow, J.-L. Bantignies, P. Dieudonné, J.-L. Sauvajol, *Angew. Chem. Int. Ed.* **2004**, *43*, 203.
[18] J. M. Ribo, J. Crusats, F. Sagues, J. Claret, R. Rubires, *Science* **2001**, *292*, 2063.
[19] A. Tsuda, M. A. Alam, T. Harada, T. Yamaguchi, N. Ishii, T. Aida, *Angew. Chem. Int. Ed.* **2007**, *46*, 8198.
[20] H. Peng, Y. T. Zhu, D. E. Peterson, Y. F. Lu, *Adv. Mater.* **2008**, *20*, 1199.
[21] K. Murata, M. Aoki, T. Suzuki, T. Harada, H. Kawabata, T. Komori, F. Ohseto, K. Ueda, S. Shinkai, *J. Am. Chem. Soc.* **1994**, *116*, 6664.
[22] Y. Zhang, P. Chen, M. Liu, *Langmuir* **2006**, *22*, 10246.
[23] P. Chen, X. Ma, M. Liu, *Macromolecules* **2007**, *40*, 4780.
[24] L. Zhang, Q. Lu, M. Liu, *J. Phys. Chem. B* **2003**, *107*, 2565.
[25] H. B. Qiu, J. J. Xie, S. Che, *Chem. Commun.* **2011**, *47*, 2607.
[26] R. Matassa, M. Carbone, R. Lauceri, R. Purrello, R. Caminiti, *Adv. Mater.* **2007**, *19*, 3961.
[27] H. Nakade, B. J. Jordan, H. Xu, G. Han, S. Srivastava, R. R. Arvizo, G. Cooke, V. M. Rotello, *J. Am. Chem. Soc.* **2006**, *128*, 14924.
[28] H. Peng, J. Tang, L. Yang, J. Pang, H. S. Ashbaugh, C. J. Brinker, Z. Yang, Y. Lu, *J. Am. Chem. Soc.* **2006**, *128*, 5304.
[29] N. C. Maiti, S. Mazumdar, N. Periasamy, *J. Phys. Chem. B* **1998**, *102*, 1528.
[30] T. Kishida, N. Fujita, K. Sada, S. Shinkai, *J. Am. Chem. Soc.* **2005**, *127*, 7298.
[31] D. L. Akins, H.-R. Zhu, C. Guo, *J. Phys. Chem.* **1994**, *98*, 3612.
[32] A. C. Ferrari, J. C. Meyer, V. Scardaci, C. Casiraghi, M. Lazzeri, F. Mauri, S. Piscanec, D. Jiang, K. S. Novoselov, S. Roth, A. K. Geim, *Phys. Rev. Lett.* **2006**, *97*, 187401.
[33] C. Casiraghia, S. Pisana, S. Novoselov, A. K. Geim, A. C. Ferrari, *Appl. Phys. Lett.* **2007**, *91*, 233108.
[34] R. A. Sidik, A. B. Anderson, N. P. Subramanian, S. P. Kumaraguru, B. N. Popov, *J. Phys. Chem. B* **2006**, *110*, 1787.
[35] L. S. Panchakarla, K. S. Subrahmanyam, S. K. Saha, A. Govindaraj, H. R. Krishnamurthy, U. V. Waghmare, C. N. R. Rao, *Adv. Mater.* **2009**, *21*, 4726.
[36] R. L. Liu, D. Q. Wu, X. L. Feng, K. Mullen, *Angew. Chem. Int. Ed.* **2010**, *49*, 2565.
[37] K. P. Gong, F. Du, Z. H. Xia, M. Durstock, L. M. Dai, *Science* **2009**, *323*, 760.